

# Application of a Hybrid Mesh-free Method Based on Generalized Finite Difference (GFD) Method for Natural Frequency Analysis of Functionally Graded Nanocomposite Cylinders Reinforced by Carbon Nanotubes

Seyed Mahmoud Hosseini<sup>1</sup>

**Abstract:** In this article, the effects of carbon nanotubes distributions on natural frequency are studied for a functionally graded nanocomposite thick hollow cylinder reinforced by single-walled carbon nanotubes using a hybrid mesh-free method. The FG nanocomposite cylinder is excited by a shock loading, which is applied on the inner surface of cylinder. The first natural frequency is obtained for various nonlinear grading patterns of distributions of the aligned carbon nanotubes. The effects of various nonlinear grading patterns on natural frequency are obtained and discussed in details. The presented hybrid mesh-free method is based on the generalized finite difference (GFD) method for spatial coordinates and Newmark finite difference (NFD) for time domain. To obtain the dynamic behavior and also first natural frequency, time histories of displacements are transferred to frequency domain by fast Fourier transformation (FFT) technique. Numerical results demonstrate the efficiency of the proposed method in frequency domain analysis for functionally graded nanocomposites reinforced by carbon nanotube (FGNRCN).

**Keywords:** Nanocomposites; Carbon nanotube; Functionally graded materials; Natural frequency; Mesh-free method; Shock loading.

## 1 Introduction

Functionally graded nanocomposites reinforced with carbon nanotubes (FGNRCN) are new kinds of composite materials, which are reinforced by carbon nanotubes with linear and nonlinear grading patterns in distribution through a certain direction. One of the most important points in designing procedure of structures made

---

<sup>1</sup> Industrial Engineering Department, Faculty of Engineering, Ferdowsi University of Mashhad, PO Box:91775-1111, Mashhad, Iran.  
Tel: +98 511 8805064 , Fax: +98 511 8763301 E-mail: sm\_hosseini@um.ac.ir

of FGNRCN is the analysis of structures under dynamic, in particular, shock loadings. When the structures are employed under dynamic and shock loading, the first natural frequency then takes place. As author known, the applications of carbon nanotubes for reinforcement of the structure and also various grading patterns in FGM have significant effect on the first natural frequency and vibration of structures. In this regards, the natural frequency analysis has a very important effect in designing procedure.

The mechanical properties of FGNRCN were presented in some researches [Esawi and Farag (2007), Thostenson, Ren and Chou (2001), Dai (2002), Lau, Gu and Hui (2006)] based on some experiments and micro mechanical models, which can be used in dynamic and vibration analysis of FGNRCN and/or single or multi wall carbon nanotubes (SWCNT or MWCNT). Zhao et al. [Zhao, Ando, Qin, Kataura, Maniwa and Saito (2002)] experimentally found radial breathing mode frequencies of multi-walled carbon nanotubes. Uchida et al. [Uchida, Tazawa, Sakai, Yamazaki and Kobayashi (2008)] experimentally deliberated on radial breathing modes of single-walled carbon nanotubes in resonance Raman spectra at high temperature and their chiral index assignment. Okada [Okada (2007)] calculated radial breathing mode frequencies of armchair nanotubes encapsulating C60 molecules (peapods). Hosseini et al. [Hosseini, Akhlaghi and Shakeri (2007)] studied the dynamic analysis of functionally graded cylinders subjected to mechanical shock loading. The mean velocity of radial stress wave propagation; natural frequency and dynamic behavior of FG cylinder were presented in their work using the Galerkin finite element (GFE) formulation with linear functionally graded elements for spatial variables and Newmark time integration scheme for time domain. For performing predefined simultaneous modification of natural frequencies and buckling loads of composite cylindrical panels, Shahab et al. [Shahab, Mirzaeifar and Bahai (2009)] proposed a new method based on the fact that both natural frequencies and buckling loads are eigenvalues of an algebraic system of simultaneous equations. An exact closed-form frequency equation is presented for free vibration analysis of circular and annular moderately thick FG plates based on the Mindlin's first-order shear deformation plate theory by Hosseini-Hashemi et al. [Hosseini-Hashemi, Fadaee and Es'haghi (2010)]. Recently, some researches were carried out by Talebian et al. [Talebian, Tahani, Hosseini and Abolbashari (2010), Talebian, Tahani, Abolbashari and Hosseini (2011), Talebian, Tahani, Abolbashari and Hosseini (2012)] in which analytical and numerical methods with high accuracy were presented to study on dynamic and natural frequency analysis in MWCNTs. A rotating CNT embedded polymer composite beam based on Euler – Bernoulli assumption with maximum centrifugal force is studied using a spectral finite element formulation by Deepak et al. [Deepak, Ganguli and Gopalakrishnan S. (2012)].

In the recent years, some meshless or mesh-free methods have been developed to solve the dynamic problems in engineering. A very short review of some recent literatures in this area that forms a background for the present study is provided as follows. A local boundary integral equation formulation in Laplace-transform domain with a meshless approximation, based on the meshless local Petrov-Galerkin (MLPG) method, was successfully implemented by Sladek et al. [Sladek, Sladek and Zhang (2003)] to solve transient elastodynamic initial-boundary value problems in continuously non-homogeneous solids. In their work, the moving least squares (MLS) method is used for interpolation and the modified fundamental solution as the test function. Daia et al. [Daia, Liua, Lima and Chen (2004)] presented a mesh-free method to analyze the static deflection and natural frequencies of thin and thick laminated composite plates using high order shear deformation theory. Two MLPG formulations based on Heaviside step functions and Gaussian weight functions were presented to analyze the dynamic behavior of elastic and elastoplastic solids by Soares Jr. et al. [Soares Jr., Sladek and Sladek (2009)]. For both their formulations, a MLS interpolation scheme was adopted, rendering a matricial time-domain system of second order ordinary differential equations. In another research, they [Soares Jr., Sladek and Sladek (2010)] used their presented method for analysis of the dynamic behavior of elastic and elastoplastic solids. Also, the propagation of thermoelastic waves in a FG thick hollow cylinder and coupled thermoelasticity analysis considering without and with Gaussian uncertainty in mechanical properties were studied by Hosseini et al. [Hosseini, Sladek, Sladek (2011), Hosseini, Shahabian, Sladek and Sladek (2011)] using meshless local Petrov-Galerkin (MLPG) method. Recently, a meshless method was developed by Moradi-dastjerdi et al. ...[Moradi-Dastjerdi, Foroutan and Pourasghar (2013)] for dynamic analysis of nanocomposite cylinders with infinite length (1D) reinforced by single-walled carbon nanotubes subjected to a mechanical loading. There are some applications for FG/NRCN such as reinforced cylindrical pressure vessels, thick cylindrical panels and cylindrical structures, which are under dynamic, impact and shock loadings. In this study, a hybrid mesh-free method based on generalized finite difference (GFD) and Newmark finite difference methods is exploited to study on the effects of various nonlinear grading patterns of carbon nanotubes distributions on natural frequency of FG/NRCN. The presented hybrid mesh-free method is applied for a thick hollow cylinder, which is reinforced by carbon nanotubes and excited by various mechanical shock loadings. The values of first natural frequency of cylinder are studied in details for various nonlinear grading patterns of distribution of nanotubes in FG/NRCN.

## 2 Mathematical formulations

### 2.1 Mechanical properties:

The mechanical properties of the FGNRCN can be obtained for a cylinder with inner radius  $r_{in}$  and outer radius  $r_{out}$  and nonlinear distributions of carbon nanotubes (CNTs) through radial direction based on a micromechanical model as follows [21]:

$$E_1 = \eta_1 V_{CN} E_1^{CN} + V_m E^m \quad (1)$$

$$\frac{\eta_2}{E_2} = \frac{V_{CN}}{E_2^{CN}} + \frac{V_m}{E^m} \quad (2)$$

$$\frac{\eta_3}{G_{12}} = \frac{V_{CN}}{G_{12}^{CN}} + \frac{V_m}{G^m} \quad (3)$$

$$v_{ij} = V_{CN} v_{ij}^{CN} + V_m v^m \quad i, j = 1, 2, 3 \quad i \neq j \quad (4)$$

$$\rho = V_{CN} \rho^{CN} + V_m \rho^m \quad (5)$$

$$V_{CN} + V_m = 1 \quad (6)$$

where  $E_1^{CN}$ ,  $E_2^{CN}$ ,  $G_{12}^{CN}$ ,  $v^{CN}$  and  $\rho^{CN}$  are elasticity modulus, shear modulus, Poisson's ratio and density of the carbon nanotubes, respectively.  $E^m$ ,  $G^m$ ,  $v^m$  and  $\rho^m$  are corresponding properties for the matrix. The terms  $V_{CN}$  and  $V_m$  are volume fractions of carbon nanotube and matrix, respectively. The subscripts CN and m stand for carbon nanotube and matrix. Three kinds of nonlinear grading patterns are assumed for carbon nanotube volume fraction as follows

$$\text{Nonlinear type } V: V_{CN} = 2 V_{CN}^* \left( \frac{r - r_{in}}{r_{out} - r_{in}} \right)^n \quad (7)$$

$$\text{Nonlinear type } \Lambda: V_{CN} = 2 V_{CN}^* \left( \frac{r_{out} - r}{r_{out} - r_{in}} \right)^n \quad (8)$$

$$\text{Nonlinear type } X: V_{CN} = 4 \eta V_{CN}^* \left( \frac{r - r_m}{r_{out} - r_{in}} \right)^n, \quad r_m = \frac{r_{out} + r_{in}}{2}, \quad (9)$$

$$\eta = \frac{r_{out} - r_{in}}{(r_{out} - r_{in})^n}$$

where

$$V_{CN}^* = \frac{\rho_m}{w_{CN} + \left( \frac{\rho_{CN}}{w_{CN}} \right) - \rho_{CN}} \quad (10)$$

The term  $w_{CN}$  is the mass fraction of nanotube. The various nonlinear grading patterns can be found for  $r_{in} = 0.5 \text{ m}$  and  $r_{out} = 1 \text{ m}$  in Figure 1.

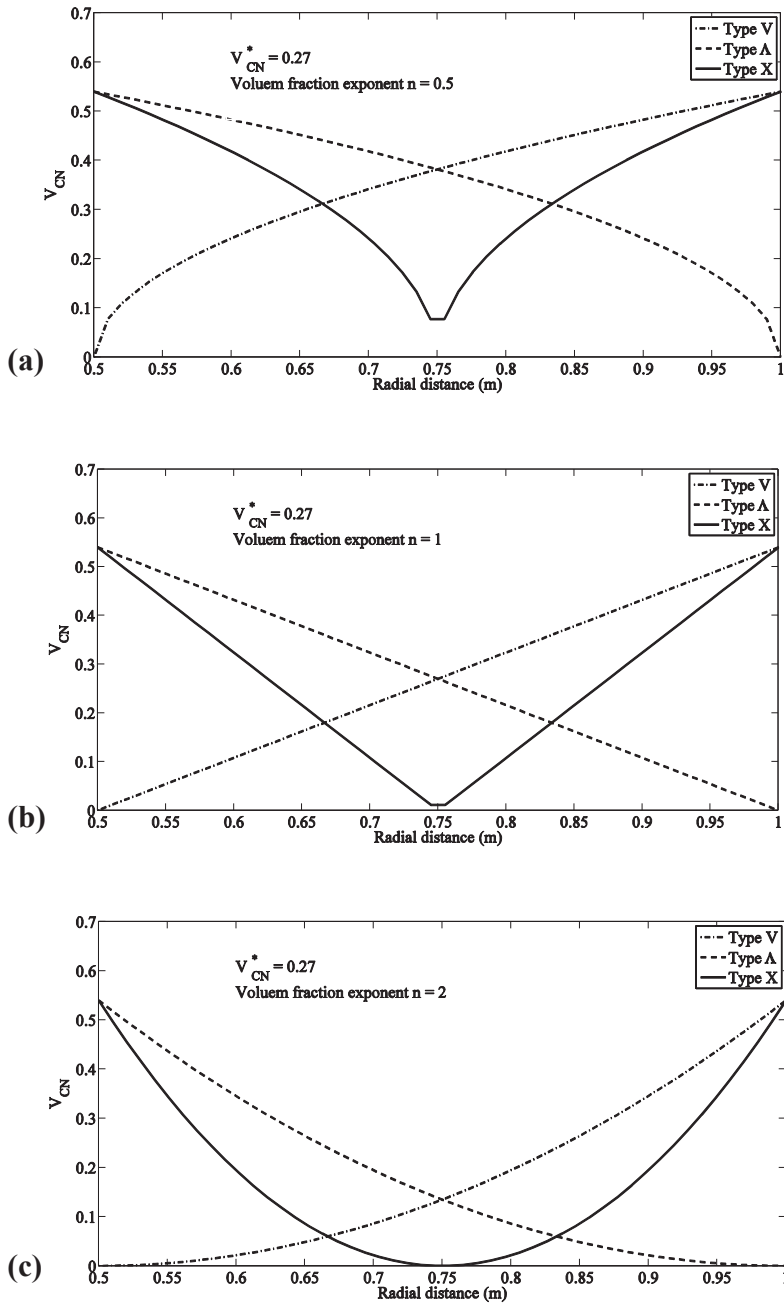


Figure 1: The distribution of volume fraction of carbon nanotube for various types of grading patterns a)  $n = 0.5$ , b)  $n = 1$ , c)  $n = 2$

## 2.2 Governing equations:

The governing equations are given as

$$\sigma_{ij,j} + f_i = \rho \ddot{u}_i \quad (11)$$

where  $f_i$ ,  $\rho$  and  $u_i$  are the body force, mass density and displacement, respectively. The constitutive equations can be found as

$$\sigma = C(r) \varepsilon, \quad \sigma_{ij} = C_{ijkl}(r) \varepsilon_{kl} \quad (12)$$

where  $\sigma_{ij}$  and  $\varepsilon_{ij}$  are the stress and strain. The matrix  $C_{ijkl}$  is defined as follows:

$$C(r) = \begin{bmatrix} C_{11}(r) & C_{12}(r) & C_{13}(r) & 0 \\ C_{12}(r) & C_{22}(r) & C_{23}(r) & 0 \\ C_{13}(r) & C_{23}(r) & C_{33}(r) & 0 \\ 0 & 0 & 0 & C_{55}(r) \end{bmatrix} \quad (13)$$

where

$$\begin{aligned} C_{11}(r) &= \frac{1 - \nu_{23}(r) \nu_{32}(r)}{E_2(r) E_3(r) \Delta}, & C_{22} &= \frac{1 - \nu_{31}(r) \nu_{13}(r)}{E_1(r) E_3(r) \Delta} \\ C_{33} &= \frac{1 - \nu_{21}(r) \nu_{12}(r)}{E_1(r) E_2(r) \Delta}, & C_{55}(r) &= G_{12}(r) \\ C_{12}(r) &= \frac{\nu_{21}(r) + \nu_{31}(r) \nu_{23}(r)}{E_2(r) E_3(r) \Delta}, & C_{23}(r) &= \frac{\nu_{32}(r) + \nu_{12}(r) \nu_{31}(r)}{E_1(r) E_3(r) \Delta} \\ C_{33}(r) &= \frac{\nu_{31}(r) + \nu_{21}(r) \nu_{32}(r)}{E_2(r) E_3(r) \Delta} \\ \Delta &= \frac{1 - \nu_{32}(r) \nu_{23}(r) - \nu_{21}(r) \nu_{12}(r) - \nu_{13}(r) \nu_{31}(r) - 2\nu_{32}(r) \nu_{21}(r) \nu_{13}(r)}{E_1(r) E_2(r) E_3(r)} \end{aligned} \quad (14)$$

The terms  $\nu_{ij}(r)$  and  $E_i(r)$  are Poisson's ratio and elasticity modulus, respectively. In this work, the body force is neglected, thus, we have

$$\sigma_{ij,j} = \rho(r) \ddot{u}_i \quad (15)$$

or

$$\sigma_{ij,j}(r,t) = \rho(r) \ddot{u}_i(r,t). \quad (16)$$

The elasticity tensor becomes

$$C_{ijkl}(r) = \frac{2\nu(r)G(r)}{1-2\nu(r)}\delta_{ij}\delta_{kl} + G(r)\delta_{ik}\delta_{jl} + G(r)\delta_{il}\delta_{jk}. \quad (17)$$

The matrix  $C_{ijkl}$  considering axisymmetry and plane strain conditions and isotropic functionally graded materials can be derived as follows.

$$C(r) = \begin{bmatrix} C_{11}(r) & C_{12}(r) \\ C_{12}(r) & C_{22}(r) \end{bmatrix} \quad (18)$$

where

$$\begin{aligned} c_{11}(r) = c_{22}(r) &= \frac{E(r)(1-\nu(r))}{(1+\nu(r))(1-2\nu(r))}, \\ c_{12}(r) = c_{21}(r) &= \frac{E(r)\nu(r)}{(1+\nu(r))(1-2\nu(r))} \end{aligned} \quad (19)$$

The following mathematical simulations are considered for mechanical properties based on micromechanical models [Shen (2009)]

$$\rho(r) = \rho_{CN} * V_{CN} + \rho_m * V_m = (\rho_{CN} - \rho_m) * V_{CN} + \rho_m \quad (20)$$

$$E(r) = E_{CN} * V_{CN} + E_m * V_m = (E_{CN} - E_m) * V_{CN} + E_m \quad (21)$$

$$\nu(r) = \nu_{CN} * V_{CN} + \nu_m * V_m = (\nu_{CN} - \nu_m) * V_{CN} + \nu_m \quad (22)$$

$$V_{CN} + V_m = 1 \quad (23)$$

The governing equation of motion can be rewritten in non-dimensional form using the following dimensionless parameters:

$$\begin{aligned} \bar{r} &= r/r_{out}, \bar{t} = tV/r_{out}, \bar{u} = u/r_{out}, \bar{E} = E/E_m \\ \bar{\rho} &= \rho/\rho_m, \bar{\sigma}_r = \sigma_r/E_m, \bar{\sigma}_\theta = \sigma_\theta/E_m \end{aligned} \quad (24)$$

where  $V$  is the velocity of elastic wave propagation in matrix. Consequently, all equations in dimensionless form are obtained as

$$\bar{\sigma}_{r,\bar{r}} + (\bar{\sigma}_r - \bar{\sigma}_\theta)/\bar{r} = \bar{\rho}(\bar{r})\bar{u}_{,\bar{t}\bar{t}} = \bar{\rho}(\bar{r})\ddot{u} \quad (25)$$

$$\bar{\sigma}_r = \bar{c}_{11}(\bar{r})\varepsilon_r + \bar{c}_{12}(\bar{r})\varepsilon_\theta \quad (26)$$

$$\bar{\sigma}_\theta = \bar{c}_{22}(\bar{r})\varepsilon_\theta + \bar{c}_{12}(\bar{r})\varepsilon_r \quad (27)$$

and

$$\varepsilon_r = \bar{u}_{,\bar{r}}, \varepsilon_\theta = \bar{u}/\bar{r} \quad (28)$$

where  $\bar{u}_{,\bar{r}} = \partial \bar{u} / \partial \bar{r}$  and

$$\bar{E}(r) = E(r)/E_m = \alpha_E V_{CN} + 1 \quad (29)$$

$$\bar{\rho}(r) = \rho(r)/\rho_m = \alpha_\rho V_{CN} + 1 \quad (30)$$

The ratios  $\alpha_E$  and  $\alpha_\rho$  are defined as follows

$$\alpha_E = E_{CN}/E_m - 1, \quad \alpha_\rho = \rho_{CN}/\rho_m - 1 \quad (31)$$

The terms  $\bar{c}_{11}(r)$  and  $\bar{c}_{12}(r)$  are

$$\alpha_1^*(\bar{r}) = \frac{(1 - \nu(r))}{(1 + \nu(r))(1 - 2\nu(r))} \quad (32)$$

$$\bar{c}_{11}(\bar{r}) = \alpha_1^*(\bar{r}) \{ \alpha_E V_{CN} + 1 \}$$

$$\alpha_2^*(\bar{r}) = \frac{\nu(r)}{(1 + \nu(r))(1 - 2\nu(r))} \quad (33)$$

$$\bar{c}_{12}(\bar{r}) = \alpha_2^*(\bar{r}) \{ \alpha_E V_{CN} + 1 \}$$

The stresses can be rewritten in the following form

$$\bar{\sigma}_r = \{ \alpha_E V_{CN} + 1 \} (\alpha_1^*(\bar{r}) \bar{u}_{,\bar{r}} + \alpha_2^*(\bar{r}) \bar{u}/\bar{r}) \quad (34)$$

$$\bar{\sigma}_\theta = \{ \alpha_E V_{CN} + 1 \} (\alpha_2^*(\bar{r}) \bar{u}_{,\bar{r}} + \alpha_1^*(\bar{r}) \bar{u}/\bar{r}) \quad (35)$$

By substituting equations (34) and (35) into (25), the dynamic governing equation in displacement form is obtained as

$$\begin{aligned} & \left\{ \alpha_E (V_{CN})_{,\bar{r}} \right\} (\alpha_1^*(\bar{r}) \bar{u}_{,\bar{r}} + \alpha_2^*(\bar{r}) \bar{u}/\bar{r}) + \\ & \alpha_1^*(\bar{r}) \{ \alpha_E V_{CN} + 1 \} (\bar{u}_{,\bar{r}\bar{r}} + (1/\bar{r}) \bar{u}_{,\bar{r}} - \bar{u}/\bar{r}^2) + \\ & \{ \alpha_E V_{CN} + 1 \} \left( (\alpha_1^*(\bar{r}))_{,\bar{r}} \bar{u}_{,\bar{r}} + (\alpha_2^*(\bar{r}))_{,\bar{r}} \bar{u}/\bar{r} \right) \\ & = \{ \alpha_\rho V_{CN} + 1 \} \bar{u}_{,\bar{t}\bar{t}} = \{ \alpha_\rho V_{CN} + 1 \} \ddot{\bar{u}} \end{aligned} \quad (36)$$

### 3 Solution technique

#### 3.1 Mesh-free generalized finite difference (GFD) method

In order to reduce the labor of creating the finite element mesh and reduce the computational cost various mesh reduction techniques were researched and developed. In the last years, some meshless and mesh-free methods were developed to solve some engineering problems. The application of meshless methods has been developed in various fields of engineering such as elastodynamic [Hosseini (2012)],

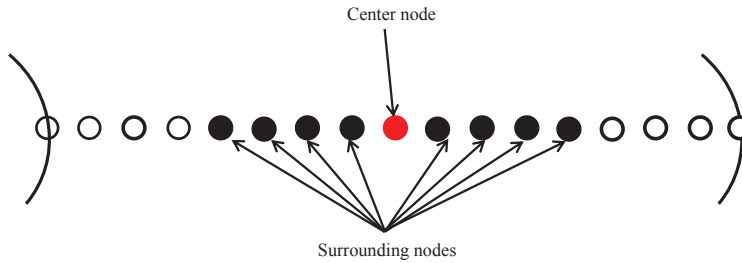


Figure 2: The sketch of center and surrounding nodes with regular distribution

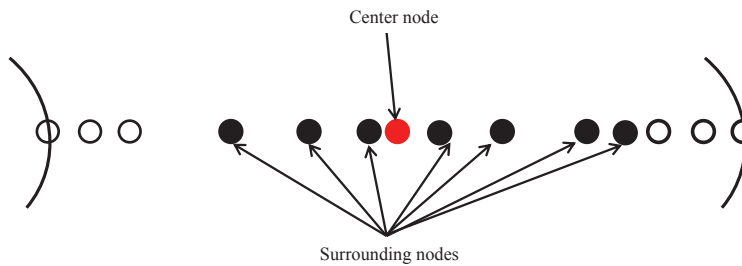


Figure 3: The sketch of center and surrounding nodes with random distribution

thermoelasticity [Hosseini, Sladek and Sladek (2011), Sladek, Sladek, Solek, Tan and Zhang (2009)], diffusion [Wu, Chang, Lu, Tao and Shen (2012)] and coupled diffusion-elasticity [Hosseini, Sladek, Sladek (2013)] and other topics. Recently, a good review was presented for analysis of problems in engineering & the sciences, with the use of the meshless methods [Sladek, Stanak, Han, Sladek and Atluri (2013)]. The success of the meshless methods lie in the local nature, as well as higher order continuity, of the trial function approximations, high adaptivity and a low cost to prepare input data for numerical analyses, since the creation of a finite element mesh is not required [Sladek, Stanak, Han, Sladek and Atluri (2009)]. Recently, the mesh-free generalized finite difference (GFD) method was developed to study on the dynamic behaviors of displacement and time history analysis in functionally graded nanocomposite cylinder reinforced by single-walled carbon nanotubes [Hosseini (2014)]. Here, the GFD method is employed to continue the presented study by author [Hosseini (2014)] for frequency domain and natural frequency analysis. The partial derivatives of displacements are linearly approximated by Taylor's series expansion on some nodes (interior nodes) in the domain. Consequently, partial derivatives are obtained at each center node i.e. the group of

nodes with a center node and surrounding other nodes is called a star in this method (see Figures 2 and 3). The nodes can be distributed on analyzed domain by regular or random distributions.

The terms  $\bar{u}_0$  and  $\bar{u}_i$  stand for the non-dimensional radial displacement at a center node and surrounding nodes, respectively. The function values  $\bar{u}_i$  can be approximated using Taylor's expansion as

$$\bar{u}_i = \bar{u}_0 + h_i (\bar{u}_0)_{,\bar{r}} + \frac{1}{2} \left[ h_i^2 (\bar{u}_0)_{,\bar{r}\bar{r}} \right] + \dots \quad (37)$$

where  $i$  denotes number of surrounding nodes. The analyzed domain in the problem is linear and through radial direction on thickness of FG cylinder. Consequently, the term  $h_i$  can be calculated as

$$h_i = \bar{r}_i - \bar{r}_o \quad (38)$$

The third and higher orders are ignored in equation (37). The norm function of non-dimensional radial displacement is minimized to decrease the error. The norm of the function for non-dimensional radial displacement is

$$Norm(\bar{u}) = \sum_{i=1}^N \left[ \left( \bar{u}_0 - \bar{u}_i + h_i (\bar{u}_0)_{,\bar{r}} + \frac{1}{2} \left[ h_i^2 (\bar{u}_0)_{,\bar{r}\bar{r}} \right] \right) w(h_i) \right]^2 \quad (39)$$

where  $w(h_i)$  is a weight function. The following weight function is employed for the problem in this article:

$$w(h_i) = 1 / (dist)^3 = 1 / h_i^3 \quad (40)$$

If the norm (39) is minimized with respect to  $\bar{u}_0$ , a set of linear equations system is obtained as follows:

$$\psi_2 Q_2 = \xi_2 \quad (41)$$

where the term  $\psi_2$  stands for  $2 \times 2$  matrices in displacement field. The components of matrices  $\psi_2$  and vector  $\xi_2$  are obtained in Appendix. The vectors  $Q_2$  is given, respectively, by

$$Q_2 = \left\{ (\bar{u}_0)_{,\bar{r}}, (\bar{u}_0)_{,\bar{r}\bar{r}} \right\}^T \quad (42)$$

There are some methods to solve the system of differential equations that one of them is Cholesky method [Benito, Urena and Gavete (2007)]. In Cholesky method, the symmetric matrix  $\psi_2$  is decomposed to upper and lower triangular matrices.

$$\psi_2 = L_2 L_2^T \quad (43)$$

The components of the matrix  $L_2$  are denoted by  $l(i, j)$  with  $i, j = 1, \dots, P$ , where  $P = 2n$  in this case, and

$$Q_2(k) = \frac{1}{l(k, k)} \left( Y(k) - \sum_{i=1}^{P-k} l(k+i, k) Q_2(k+i) \right) \quad (k = 1, \dots, P) \quad (44)$$

$$Y(k) = \left( -\bar{u}_0 \sum_{i=1}^P M(k, i) c_i + \sum_{j=1}^N \bar{u}_j \left( \sum_{i=1}^P M(k, i) d_{ji} \right) \right) \quad (k = 1, \dots, P) \quad (45)$$

$$M(i, j) = (-1)^{i+j} \frac{1}{l(i, j)} \sum_{k=j}^{i-1} l(i, j) M(k, j) \quad \text{with } j < i \quad (i, j = 1, \dots, P) \quad (46)$$

$$M(i, j) = \frac{1}{l(i, j)} \quad \text{with } j = i \quad (i, j = 1, \dots, P) \quad (47)$$

$$M(i, j) = 0 \quad \text{with } j > i \quad (i, j = 1, \dots, P) \quad (48)$$

For this problem, it becomes

$$c_i = \sum_{j=1}^N d_{ji}, \quad d_{j1} = h_j W^2, \quad d_{j2} = (h_i^2/2) W^2 \quad (49)$$

where

$$W^2 = (w(h_i))^2 \quad (50)$$

Also, the first and second derivatives of non-dimensional radial displacement can be calculated as

$$(\bar{u}_0)_{,\bar{r}} = A_1^u \left\{ \sum_{i=1}^N (-\bar{u}_0 + \bar{u}_i) h_i w^2(h_i) \right\} - A_2^u \left\{ \sum_{i=1}^N (-\bar{u}_0 + \bar{u}_i) (h_i^2/2) w^2(h_i) \right\} \quad (51)$$

$$(\bar{u}_0)_{,\bar{r}\bar{r}} = B_1^u \left\{ \sum_{i=1}^N (-\bar{u}_0 + \bar{u}_i) h_i w^2(h_i) \right\} - B_2^u \left\{ \sum_{i=1}^N (-\bar{u}_0 + \bar{u}_i) (h_i^2/2) w^2(h_i) \right\} \quad (52)$$

where the coefficients  $A_1^u$ ,  $A_2^u$ ,  $B_1^u$  and  $B_2^u$  are obtained in details in Appendix. The derivatives of radial displacement can be also rewritten in star forms as follow

$$(\bar{u}_0)_{,\bar{r}} = -\alpha_0 \bar{u}_0 + \sum_{i=1}^N \alpha_i \bar{u}_i \quad (53)$$

where

$$\begin{aligned}\alpha_i &= A_1^u h_i^2 w^2(h_i) - A_2^u (h_i^2/2) w^2(h_i) \\ \alpha_0 &= \sum_{i=1}^N \alpha_i\end{aligned}\quad (54)$$

The second derivative of radial displacement can be written as

$$(\bar{u}_0)_{,\bar{r}\bar{r}} = -\beta_0 \bar{u}_0 + \sum_{i=1}^N \beta_i \bar{u}_i \quad (55)$$

where

$$\begin{aligned}\beta_i &= B_1^u h_i^2 w^2(h_i) - B_2^u (h_i^2/2) w^2(h_i) \\ \beta_0 &= \sum_{i=1}^N \beta_i\end{aligned}\quad (56)$$

The first and second derivatives of non-dimensional radial displacement are replaced by obtained relations in star forms in equation (26), which is defined for a center node. The governing equation should be valid at every center node on analyzed domain such as  $\bar{r}_0$ :

$$\begin{aligned}& \left\{ \alpha_E (V_{CN})_{,\bar{r}} \right\} \left( \alpha_1^*(\bar{r}) (\bar{u}_0)_{,\bar{r}} + \alpha_2^*(\bar{r}) \bar{u}_0 / \bar{r}_0 \right) + \\ & \alpha_1^*(\bar{r}) \left\{ \alpha_E V_{CN} + 1 \right\} \left( (\bar{u}_0)_{,\bar{r}\bar{r}} + (1/\bar{r}_0) (\bar{u}_0)_{,\bar{r}} - \bar{u}_0 / \bar{r}_0^2 \right) + \\ & \left\{ \alpha_E V_{CN} + 1 \right\} \left( (\alpha_1^*(\bar{r}))_{,\bar{r}} (\bar{u}_0)_{,\bar{r}} + (\alpha_2^*(\bar{r}))_{,\bar{r}} \bar{u}_0 / \bar{r}_0 \right) \\ & = \left\{ \alpha_\rho V_{CN} + 1 \right\} \ddot{u}_0\end{aligned}\quad (57)$$

$$\begin{aligned}& \left\{ \alpha_E (V_{CN})_{,\bar{r}} \right\} \left( \alpha_1^*(\bar{r}_0) \left( -\alpha_0 \bar{u}_0 + \sum_{i=1}^N \alpha_i \bar{u}_i \right) + \alpha_2^*(\bar{r}_0) \bar{u}_0 / \bar{r}_0 \right) + \\ & \alpha_1^*(\bar{r}_0) \left\{ \alpha_E V_{CN} + 1 \right\} \left[ \left( -\beta_0 \bar{u}_0 + \sum_{i=1}^N \beta_i \bar{u}_i \right) + (1/\bar{r}_0) \left( -\alpha_0 \bar{u}_0 + \sum_{i=1}^N \alpha_i \bar{u}_i \right) - \bar{u}_0 / \bar{r}_0^2 \right] + \\ & \left\{ \alpha_E V_{CN} + 1 \right\} \left[ (\alpha_1^*(\bar{r}_0))_{,\bar{r}} \left( -\alpha_0 \bar{u}_0 + \sum_{i=1}^N \alpha_i \bar{u}_i \right) + (\alpha_2^*(\bar{r}_0))_{,\bar{r}} \bar{u}_0 / \bar{r}_0 \right] \\ & = \left\{ \alpha_\rho V_{CN} + 1 \right\} \ddot{u}_0\end{aligned}\quad (58)$$

where

$$\bar{u}_0 = \bar{u}(\bar{r}_0) \quad (59)$$

Also, the above equation can be rewritten as

$$\begin{aligned}
 & \left[ \left\{ \alpha_E (V_{CN})_{,\bar{r}} \right\} (\alpha_2^*(\bar{r}_0)/\bar{r}_0 - \alpha_1^*(\bar{r}_0) \alpha_0) - \right. \\
 & \alpha_1^*(\bar{r}_0) \left\{ \alpha_E V_{CN} + 1 \right\} (\beta_0 + \alpha_0/\bar{r}_0 + 1/\bar{r}_0^2) + \\
 & \left. \left\{ \alpha_E V_{CN} + 1 \right\} \left( (\alpha_2^*(\bar{r}_0))_{,\bar{r}} 1/\bar{r}_0 - (\alpha_1^*(\bar{r}_0))_{,\bar{r}} \alpha_0 \right) \right] \bar{u}_0 + \\
 & \sum_{i=1}^N \left[ \left\{ \alpha_E (V_{CN})_{,\bar{r}} \right\} \alpha_1^*(\bar{r}_0) \alpha_i + \alpha_1^*(\bar{r}_0) \left\{ \alpha_E V_{CN} + 1 \right\} (\beta_i + \alpha_i/\bar{r}_0) + \right. \\
 & \left. \left\{ \alpha_E V_{CN} + 1 \right\} (\alpha_1^*(\bar{r}_0))_{,\bar{r}} \alpha_i \right] \bar{u}_i = \left\{ \alpha_\rho V_{CN} + 1 \right\} \ddot{u}_0
 \end{aligned} \tag{60}$$

The following system of linear equations is obtained for the distributed nodes on the analyzed domain.

$$[M]_{(N+1)*(N+1)} \{\ddot{\varphi}\}_{(N+1)*1} + [K]_{(N+1)*(N+1)} \{\varphi\}_{(N+1)*1} = [f]_{(N+1)*1} \tag{61}$$

where

$$\{\varphi\}^T = \left\{ \bar{u}_0 \quad \bar{u}_1 \quad . \quad . \quad . \quad \bar{u}_N \quad \right\}^T \tag{62}$$

and

$$\{\ddot{\varphi}\}^T = \left\{ \ddot{u}_0 \quad \ddot{u}_1 \quad . \quad . \quad . \quad \ddot{u}_N \quad \right\}^T \tag{63}$$

### 3.2 Newmark finite difference (NFD) method

In this article, the Newmark time approximation scheme with suitable time step is used, and the time-dependent displacement field is obtained for the cylinder. Consider the system to be expressed in terms of non-dimensional time  $\bar{t} = t_p$  in which the governing equation of system takes the form

$$[M] \{\ddot{\varphi}^{t_p}\} + [K] \{\varphi^{t_p}\} = [f^{t_p}] \tag{64}$$

Using the initial conditions  $\{f^0\}$  and  $\{\varphi^0\}$ , the following equation can be obtained

$$[M] \{\ddot{\varphi}^0\} = \{f^0\} - [K] \{\varphi^0\} \tag{65}$$

The matrices  $[K_m]$  and  $\{f_m^{t_p}\}$  are defined as follows:

$$[K_m] = [K] + \frac{1}{\lambda_1 \Delta t^2} [M] \tag{66}$$

$$\{f_m^{t_p}\} = \{f^{t_p}\} + \frac{1}{\lambda_1 \Delta t^2} [M] (\{\phi^{t_{p-1}}\} + \Delta t \{\dot{\phi}^{t_{p-1}}\} + (0.5 - \lambda_1) \Delta t^2 \{\ddot{\phi}^{t_{p-1}}\}) \quad (67)$$

The matrices of  $[\phi^{t_p}]$ ,  $[\dot{\phi}^{t_p}]$ , and  $[\ddot{\phi}^{t_p}]$  can be computed using following equations:

$$\{\phi^{t_p}\} = [K_m]^{-1} \{f_m^{t_p}\} \quad (68)$$

$$\{\dot{\phi}^{t_p}\} = \frac{1}{\lambda_1 \Delta t^2} (\{\phi^{t_p}\} - \{\phi^{t_{p-1}}\} - \Delta t \{\dot{\phi}^{t_{p-1}}\} - \Delta t^2 (0.5 - \lambda_1) \{\ddot{\phi}^{t_{p-1}}\}) \quad (69)$$

$$\{\ddot{\phi}^{t_p}\} = \{\dot{\phi}^{t_{p-1}}\} + \Delta t [(1 - \lambda_2) \{\ddot{\phi}^{t_{p-1}}\} + \lambda_2 \{\dot{\phi}^{t_p}\}] \quad (70)$$

Using aforementioned equations, the matrices of  $[\phi^{t_p}]$ ,  $[\dot{\phi}^{t_p}]$ , and  $[\ddot{\phi}^{t_p}]$  can be obtained for an arbitrary time. The best convergence rate can be achieved in this method by choosing  $\lambda_1 = \frac{1}{4}$  and  $\lambda_2 = \frac{1}{2}$ .

### 3.3 Fast Fourier transformation (FFT)

To find the natural frequencies, the dynamic response of displacement in time domain, which is based on shock loading, should be transferred to frequency domain. The fast Fourier transformation (FFT) technique is employed for this purpose. The discrete data can be transferred from time domain into frequency domain using following equation.

$$\bar{U}_K(\bar{r}, \bar{w}) = \sum_{\tau=0}^{N_t-1} \bar{u}_\tau(\bar{r}, \bar{t}) e^{-\frac{2\pi i}{N_t} \tau K} \quad K = 0, \dots, N_t - 1 \quad (71)$$

where “ $\bar{U}_K$ ”, “ $N_t$ ” and “ $\bar{w}$ ” are non-dimensional radial displacement at frequency domain, number of sample nodes that are transferred from time to frequency domain and non-dimensional frequency. The process time of the discrete Fourier transformation (71) can be decreased by dividing the vector “ $\bar{u}_\tau(\bar{r}, \bar{t})$ ” to two vectors in even and odd counters as follow.

$$\begin{aligned} \bar{U}_K(\bar{r}, \bar{w}) &= \sum_{\tau=0}^{N_t-1} \bar{u}_\tau(\bar{r}, \bar{t}) e^{-\frac{2\pi i}{N_t} \tau K} \\ &= \sum_{\tau=0}^{N_t/2-1} \bar{u}_{2\tau}(\bar{r}, \bar{t}) e^{-\frac{2\pi i}{N_t} (2\tau) K} + \sum_{\tau=0}^{N_t/2-1} \bar{u}_{2\tau+1}(\bar{r}, \bar{t}) e^{-\frac{2\pi i}{N_t} (2\tau+1) K} \end{aligned} \quad (72)$$

$$\begin{aligned}
\bar{U}_K(\bar{r}, \bar{w}) &= \sum_{\tau=0}^{N_t-1} \bar{u}_n(\bar{r}, \bar{t}) e^{-\frac{2\pi i}{N_t} \tau K} \\
&= \sum_{\tau=0}^{N_t/2-1} \bar{u}_{2\tau}(\bar{r}, \bar{t}) e^{-\frac{2\pi i}{N_t} (2\tau) K} + \sum_{\tau=0}^{N_t/2-1} \bar{u}_{2\tau+1}(\bar{r}, \bar{t}) e^{-\frac{2\pi i}{N_t} (2\tau+1) K} \\
&= \sum_{\tau=0}^{N_t/2-1} \bar{u}_{2\tau}^{even}(\bar{r}, \bar{t}) e^{-\frac{2\pi \cdot i \cdot \tau \cdot K}{N_t/2}} + e^{-\frac{2\pi \cdot i \cdot K}{N_t}} \sum_{\tau=0}^{N_t/2-1} \bar{u}_{2\tau}^{odd}(\bar{r}, \bar{t}) e^{-\frac{2\pi \cdot i \cdot \tau \cdot K}{N_t/2}}
\end{aligned} \tag{73}$$

Using aforementioned algorithm, the number of process in Fourier transformation technique can be decreased from “ $2N_t^2$ ” to “ $2N_t \log_2 N_t$ ”.

#### 4 Numerical example and discussions

Consider a cylinder with inner radius  $\bar{r}_{in}$  and outer radius  $\bar{r}_{out}$  made of functionally graded nanocomposites reinforced by carbon nanotube (FGNRCN). The term  $H$  is defined as  $H = \bar{r}_{out} - \bar{r}_{in}$ . Suddenly unloading on inner bounding surface of cylinder in a certain time can be considered as a mechanical shock loading. So, the following boundary conditions are considered as first example for the problem to derive the time histories of non-dimensional radial displacement:

$$\sigma_r(r_{in}, t) = P_0 t [1 - H(t - t_0)] \tag{74}$$

$$\sigma_r(r_{out}, t) = 0 \tag{75}$$

where

$$r_{in} = 1m, \quad r_{out} = 1.5m, \quad t_0 = 0.005 \text{ sec}, \quad P_0 = -4 \text{ Gpa/sec}$$

and the function  $H(t - t_0)$  is Heaviside unit step function. To validate the presented solving method, the mechanical properties of FGNRCN are considered to be equal with full aluminum cylinder (isotropic cylinder by employing  $n = 0$ ). So, the dynamic behaviors can be compared to those presented by Hosseini et al. [Hosseini, Akhlaghi and Shakeri (2007)]. Figure 4 shows a comparison in radial displacement between obtained results by the presented hybrid mesh-free method and finite element method. A good agreement can be observed in Figure 4 for the results obtained by presented method. The time histories of radial displacement at  $r = r_{in} + H/2$  are illustrated in Figure 5 for various kinds of grading patterns,  $V_{CN}^* = 0.17$  and FG type V. The presented time histories in Figure 5 are transferred to frequency domain employing FFT technique. The dynamic behaviors in frequency domain can be found in Figure 6 in which the frequencies of each peak

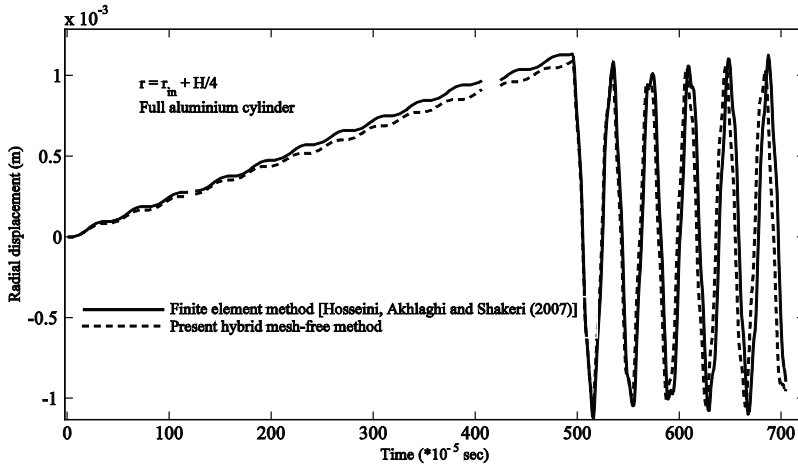


Figure 4: The comparison between obtained results from presented mesh-free method and those from finite element method by Hosseini et al. [Hosseini, Akhlaghi and Shakeri (2007)]

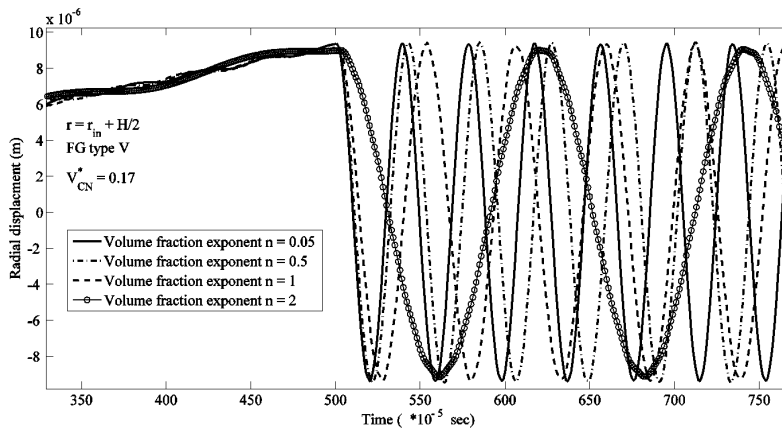


Figure 5: The time histories of radial displacement for various values of  $n$  at  $r = r_{in} + H/2$  for FG type V and  $V_{CN}^* = 0.17$  in first example

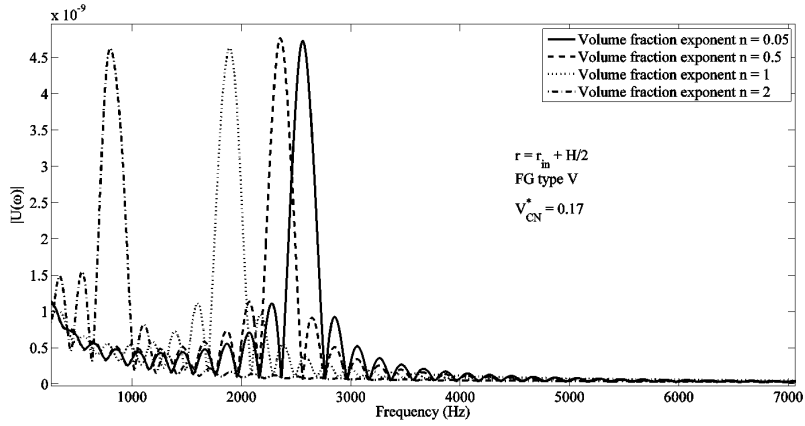


Figure 6: Frequency domain for various values of  $n$ ,  $V_{CN}^* = 0.17$  and FG type V in first example

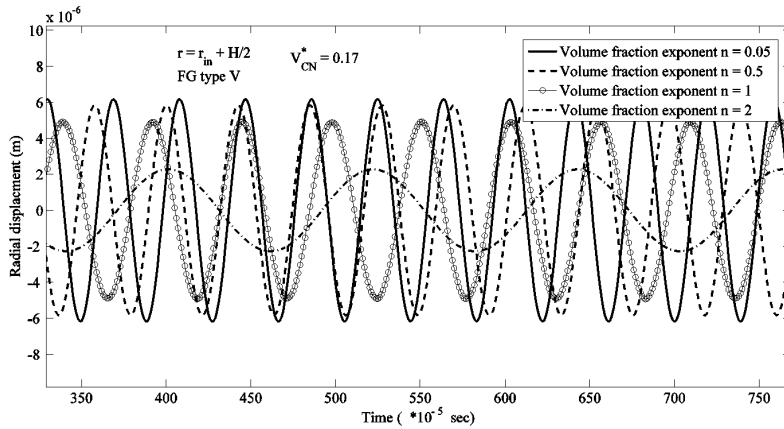


Figure 7: The time histories of radial displacement for various values of  $n$  at  $r = r_{in} + H/2$  for FG type V and  $V_{CN}^* = 0.17$  in second example

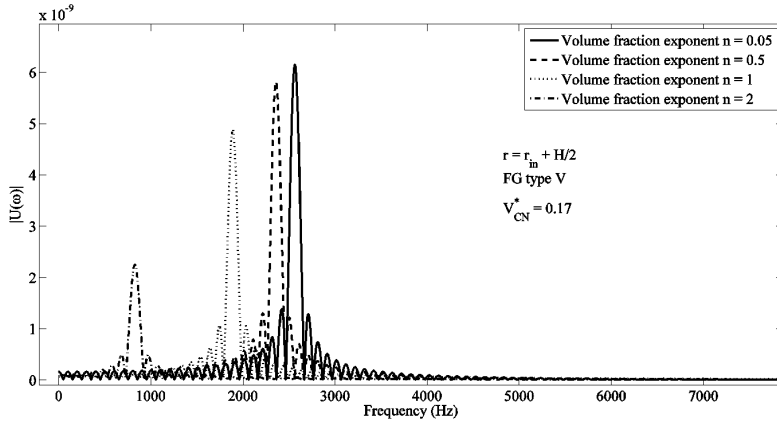


Figure 8: Frequency domain for various values of  $n$ ,  $V_{CN}^* = 0.17$  and FG type V in second example

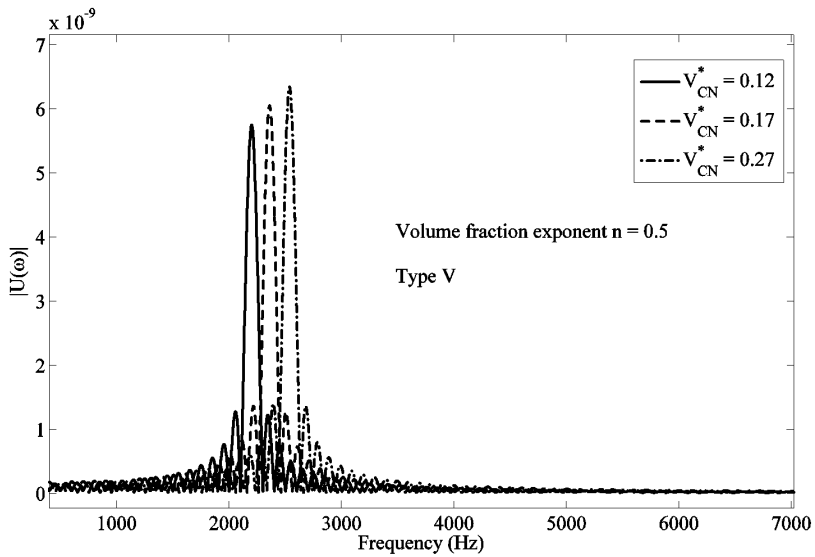


Figure 9: Frequency domain for various values of  $V_{CN}^*$  and  $n = 0.5$  in FG type V

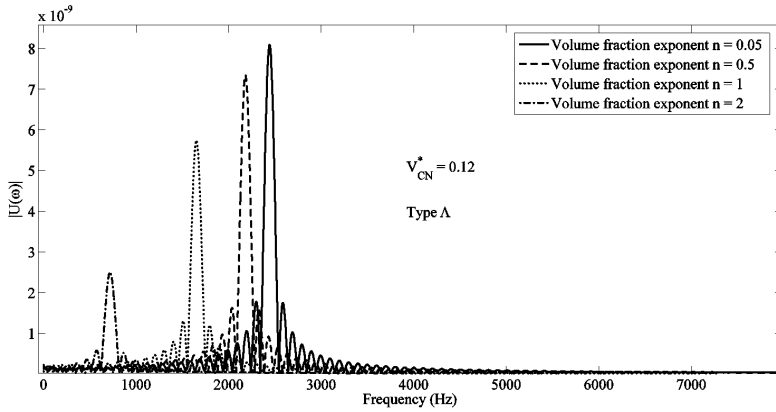


Figure 10: Frequency domain for various values of  $n$  and  $V_{CN}^* = 0.12$  in FG type  $\Lambda$

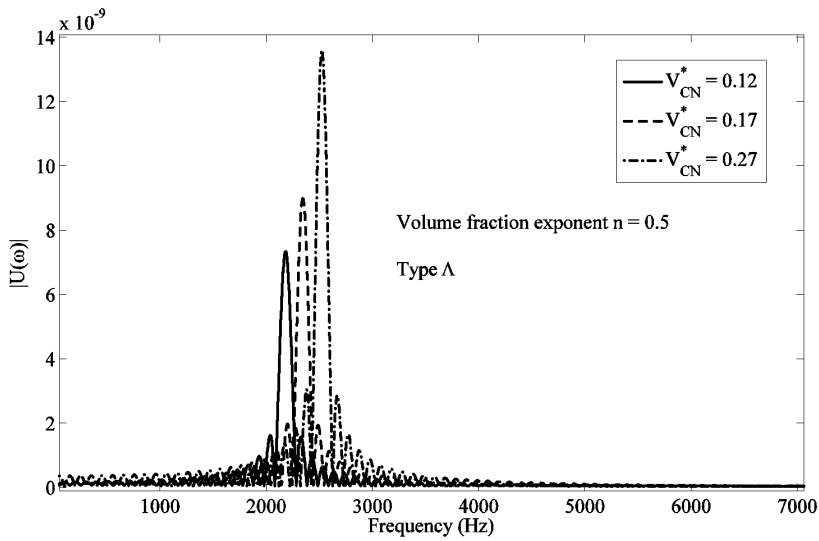


Figure 11: Frequency domain for various values of  $V_{CN}^*$  and  $n = 0.5$  in FG type  $\Lambda$

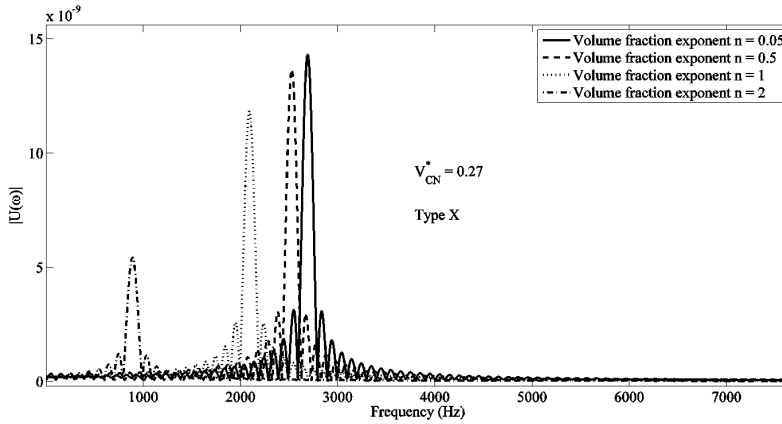


Figure 12: Frequency domain for various values of  $n$  and  $V_{CN}^* = 0.27$  in FG type X

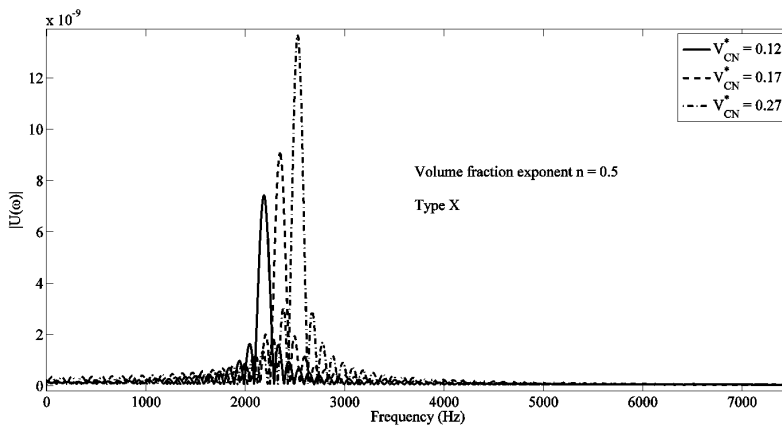


Figure 13: Frequency domain for various values of  $V_{CN}^*$  and  $n = 0.5$  in FG type X

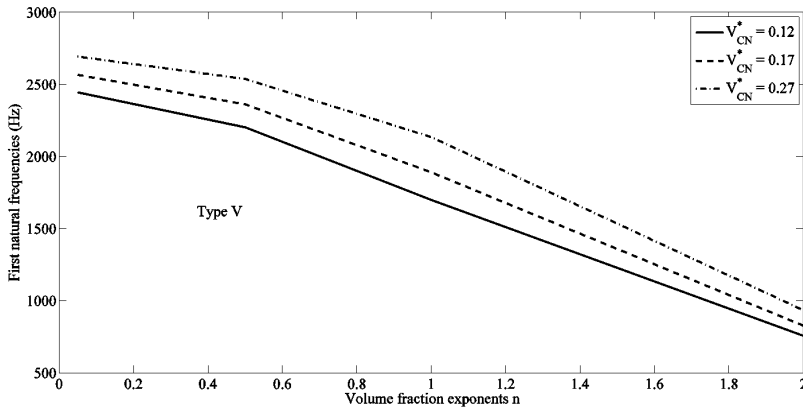


Figure 14: Variation of first natural frequencies versus  $n$  for various values of  $V_{CN}^*$  in FG type V

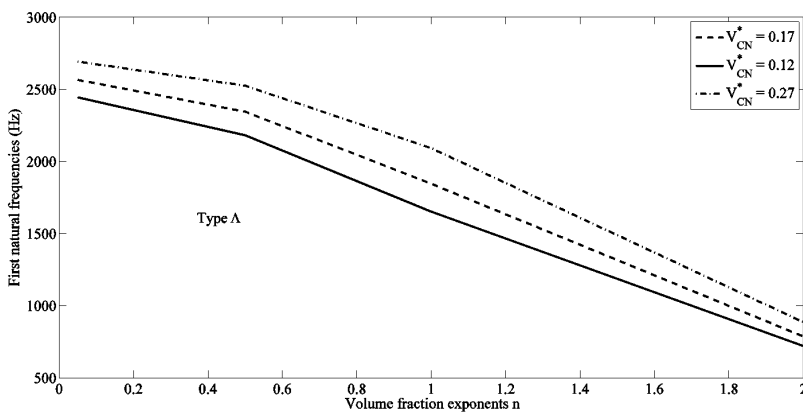


Figure 15: Variation of first natural frequencies versus  $n$  for various values of  $V_{CN}^*$  in FG type A

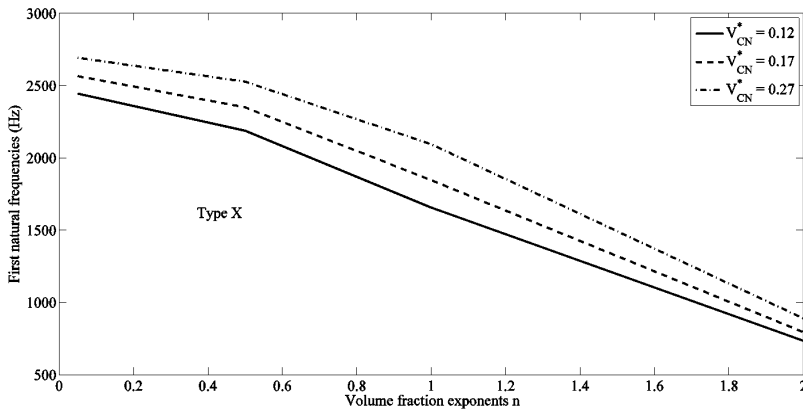


Figure 16: Variation of first natural frequencies versus  $n$  for various values of  $V_{CN}^*$  in FG type X

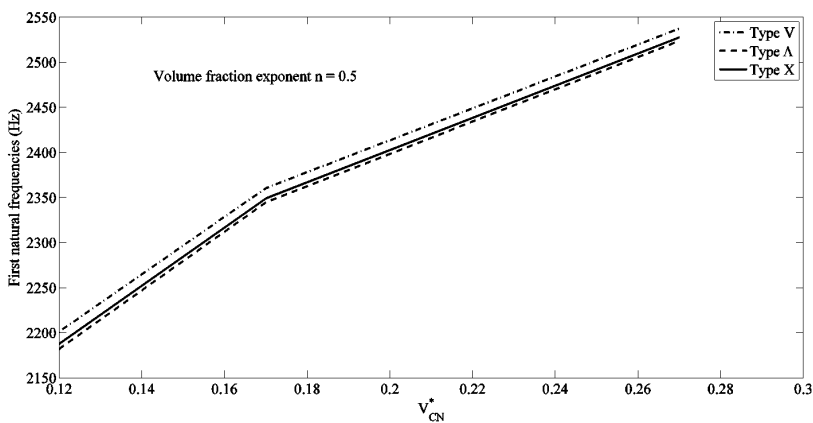


Figure 17: Variation of first natural frequencies versus  $V_{CN}^*$  for various types of FGRCN and  $n = 0.5$

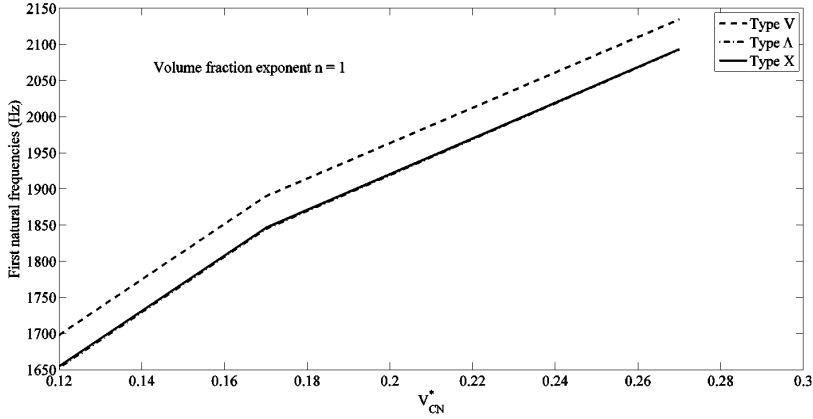


Figure 18: Variation of first natural frequencies versus  $V_{CN}^*$  for various types of FGNNRCN and  $n = 1$

point depict the first natural frequencies of FGNNRCN. As second example, the following boundary conditions are considered for the problem.

$$\sigma_r(r_{in}, t) = P_0 \sin\left(\frac{\pi t}{t_0}\right) \quad (76)$$

$$\sigma_r(r_{out}, t) = 0 \quad (77)$$

where

$$r_{in} = 1 \text{ m} , \quad r_{out} = 1.5 \text{ m} , \quad t_0 = 0.00015 \text{ sec} , \quad P_0 = -10 \text{ Mpa}$$

The time histories of radial displacement are given for various grading patterns at  $r = r_{in} + H/2$ ,  $V_{CN}^* = 0.17$  and FG type V in Figure 7 as the same with Figure 5. Using FFT technique, all of time histories are transferred to frequency domain, which are shown in Figure 8. The first natural frequencies of FGNNRCN, which are obtained from Figure 8, are the same with those obtained from Figure 6. It can be considered as another verification of presented method to obtain first natural frequencies. To find the first natural frequencies, the FGNNRCN should be excited by a mechanical shock loading. The kind of shock loading is not important for the analysis. It is concluded from Figure 8 when the values of  $n$  are increased the first natural frequency is decreased. The effects of various values of  $V_{CN}^*$  on first natural frequencies for  $n = 0.5$  and FG type V can be found in Figure 9. The first natural frequencies are increased when the values of  $V_{CN}^*$  are increased. By considering

the FG type  $\Lambda$  for FGNNRCN, the effects of variation in values of  $n$  and  $V_{CN}^*$  on first natural frequencies can be found in Figures 10 and 11, respectively. The same behaviors can be observed in Figures 10 and 11 comparing to Figures 8 and 9. Also, similar effects on first natural frequencies are obtained for FG type X, which are illustrated in Figures 12 and 13.

The variations of first natural frequencies versus volume fraction exponents  $n$  for various values of  $V_{CN}^*$  are drawn for FG type V,  $\Lambda$  and X in Figures 14, 15 and 16, respectively. In all kinds of FGNNRCN and all values of  $V_{CN}^*$ , it is concluded when the value of  $n$  is increased the value of first natural frequency is decreased as a nonlinear function. Figures 17 and 18 show us the variation of first natural frequency versus  $V_{CN}^*$  for various kinds of FGNNRCN for  $n = 0.5$  and  $n = 1$ , respectively. It is concluded from Figures 14 to 18 that in all kinds of FGNNRCN the first natural frequency is increased by increasing the value of  $V_{CN}^*$ . The values of first natural frequency for some certain values of volume fraction exponents  $n$  including  $n = 0.05$ ,  $n = 0.5$ ,  $n = 1$  and  $n = 2$  and some certain values of  $V_{CN}^*$  such as  $V_{CN}^* = 0.12$ ,  $V_{CN}^* = 0.17$  and  $V_{CN}^* = 0.27$  are shown for FG type V,  $\Lambda$  and X in Table 1. In all kinds of FGNNRCN and all values of  $V_{CN}^*$ , it is concluded when the value of  $n$  is increased the value of first natural frequency is decreased as a nonlinear function. By using the presented diagrams in Figures 14 to 18, it is possible to approximate the values of natural frequency for other values of  $n$  and  $V_{CN}^*$ , which are not presented in Table 1.

Table 1: First natural frequencies (Hz) of FGNNRCN

	Type V			Type $\Lambda$			Type X		
	$V_{CN}^*$			$V_{CN}^*$			$V_{CN}^*$		
	0.12	0.17	0.27	0.12	0.17	0.27	0.12	0.17	0.27
$n = 0.05$	2444	2565.85	2692.4	2442.7	2564.8	2691.65	2443.3	2565.3	2692
$n = 0.5$	2201	2360.45	2537.25	2182	2344.5	2523.7	2187.9	2349.2	2527.6
$n = 1$	1697.8	1890	2134.7	1652.2	1844.8	2093	1654.8	1846.2	2093.2
$n = 2$	756	827.4	933.75	719.4	785.5	886.45	734.85	795.6	889.62

## 5 Conclusions

In this paper, a hybrid mesh-free method based on mesh-free generalized finite difference (GFD) method and Newmark finite difference (NFD) method is developed for natural frequency analysis in a functionally graded nanocomposite reinforced by carbon nanotubes (FGNNRCN) subjected to mechanical shock loading. The distribution of carbon nanotubes in FG nanocomposite are considered to vary as nonlinear

function of radius, which varies with various nonlinear grading patterns continuously through radial direction. The effective material properties of functionally graded carbon nanotube are estimated using a micro-mechanical model. The main contributions of this paper can be summarized as follows.

- The mechanical shock analysis of FGRCN thick hollow cylinder is carried out and the dynamic behavior of displacement field and the time history of radial displacement are obtained for two kinds of mechanical shock loading.
- The first natural frequencies of FGRCN are obtained for various grading patterns and kinds of FG nanocomposites.
- An effective hybrid mesh-free method based on generalized finite difference (GFD) and Newmark finite difference (NFD) methods is presented to calculate the first natural frequency of FGRCN.
- The effects of various grading patterns and various kinds of FG types in FG nanocomposites on first natural frequency of FGRCN are studied in details using presented mesh-free method.
- The first natural frequencies are calculated and reported for three kinds of FG nanocomposite with various nonlinear grading patterns.

The presented hybrid mesh-free method has a high capability for dynamic analysis and natural frequency assessment and also for calculating the first natural frequency in a FGRCN.

## Appendix

The first and second derivations of non-dimensional radial can be calculated as follows.

$$\left[ \begin{array}{cc} \sum_{i=1}^N h_i^2 w^2(h_i) & \sum_{i=1}^N \frac{h_i^3}{2} w^2(h_i) \\ \sum_{i=1}^N \frac{h_i^3}{2} w^2(h_i) & \sum_{i=1}^N \frac{h_i^4}{4} w^2(h_i) \end{array} \right] \left\{ \begin{array}{c} \frac{\partial \bar{u}_0}{\partial \bar{r}} \\ \frac{\partial^2 \bar{u}_0}{\partial \bar{r}^2} \end{array} \right\} = \left[ \begin{array}{c} \sum_{i=1}^N (-\bar{u}_0 + \bar{u}_i) h_i w^2(h_i) \\ \sum_{i=1}^N (-\bar{u}_0 + \bar{u}_i) \frac{h_i^2}{2} w^2(h_i) \end{array} \right] \quad (\text{A1})$$

The first and second derivatives are presented by equations (11) and (12), which

the unknown coefficients can be calculated as follows:

$$A_1^u = \frac{\left( \sum_{i=1}^N \frac{h_i^4}{4} w^2(h_i) \right)}{\left( \sum_{i=1}^N h_i^2 w^2(h_i) \right) \left( \sum_{i=1}^N \frac{h_i^4}{4} w^2(h_i) \right) - \left( \sum_{i=1}^N \frac{h_i^3}{2} w^2(h_i) \right)^2} \quad (\text{A2})$$

$$A_2^u = \frac{\left( \sum_{i=1}^N \frac{h_i^3}{2} w^2(h_i) \right)}{\left( \sum_{i=1}^N h_i^2 w^2(h_i) \right) \left( \sum_{i=1}^N \frac{h_i^4}{4} w^2(h_i) \right) - \left( \sum_{i=1}^N \frac{h_i^3}{2} w^2(h_i) \right)^2} \quad (\text{A3})$$

$$B_1^u = \frac{-\left( \sum_{i=1}^N \frac{h_i^3}{2} w^2(h_i) \right)}{\left( \sum_{i=1}^N h_i^2 w^2(h_i) \right) \left( \sum_{i=1}^N \frac{h_i^4}{4} w^2(h_i) \right) - \left( \sum_{i=1}^N \frac{h_i^3}{2} w^2(h_i) \right)^2} \quad (\text{A4})$$

$$B_2^u = \frac{-\left( \sum_{i=1}^N h_i^2 w^2(h_i) \right)}{\left( \sum_{i=1}^N h_i^2 w^2(h_i) \right) \left( \sum_{i=1}^N \frac{h_i^4}{4} w^2(h_i) \right) - \left( \sum_{i=1}^N \frac{h_i^3}{2} w^2(h_i) \right)^2} \quad (\text{A5})$$

## References

- Benito, J. J.; Urena, F.; Gavete, L.** (2007): Solving parabolic and hyperbolic equations by the generalized finite difference method. *J Comput Appl Math*, vol. 209, pp. 208-233.
- Dai, H.** (2002): Carbon nanotubes: opportunities and challenges. *Surface Sciences*, vol. 500, pp. 218-41.
- Daia, K. Y.; Liua, G. R.; Lima, K. M.; Chen, X. L.** (2004): A mesh-free method for static and free vibration analysis of shear deformable laminated composite plates. *Journal of Sound and Vibration*, vol. 269, pp. 633-652.
- Deepak, B. P.; Ganguli, R.; Gopalakrishnan, S.** (2012): Dynamics of rotating composite beams: A comparative study between CNT reinforced polymer composite beams and laminated composite beams using spectral finite elements. *International Journal of Mechanical Sciences*, vol. 64, pp. 110-126.
- Esawi, A. M. K.; Farag, M. M.** (2007): Carbon nanotube reinforced composites: potential and current challenges. *Materials and Design*, vol. 28, pp. 2394-401.
- Hosseini, S. M.; Akhlaghi, M.; Shakeri, M.** (2007): Dynamic response and radial wave propagation velocity in thick hollow cylinder made of functionally graded materials. *Engineering Computations*, vol. 24, no. 3, pp. 288-303.

- Hosseini, S. M.; Sladek, J.; Sladek, V.** (2011): Meshless local Petrov-Galerkin method for coupled thermoelasticity analysis of a functionally graded thick hollow cylinder. *Engineering Analysis with Boundary Element*, vol. 35, no. 6, pp. 827-835.
- Hosseini, S. M.; Shahabian, F.; Sladek, J.; Sladek, V.** (2011): Stochastic Meshless Local Petrov-Galerkin (MLPG) Method for Thermo-Elastic Wave Propagation Analysis in Functionally Graded Thick Hollow Cylinders. *CMES: Computer Modeling in Engineering & Sciences*, vol. 71, no. 1, pp. 39-66.
- Hosseini, S. M.** (2012): Analysis of elastic wave propagation in a functionally graded thick hollow cylinder using a hybrid mesh-free method. *Eng. Anal. Bound. Elem.*, Vol. 36, pp.1536–1545.
- Hosseini, S. M.; Sladek, J.; Sladek, V.** (2013) Application of meshless local integral equations to two dimensional analysis of coupled non-Fick diffusion–elasticity. *Eng. Anal. Bound. Elem.*, vol. 37, pp. 603-615.
- Hosseini, S. M.** (2014): Elastic wave propagation and time history analysis in functionally graded nanocomposite cylinders reinforced by carbon nanotubes using a hybrid mesh-free method. *Engineering Computations* (Accepted for publication).
- Hosseini-Hashemi, Sh.; Fadaee, M.; Es’haghi, M.** (2010): A novel approach for in-plane/out-of-plane frequency analysis of functionally graded circular/annular plates. *International Journal of Mechanical Sciences*, vol. 52, pp. 1025–1035.
- Lau, K. T.; Gu, C.; Hui, D.** (2006): A critical review on nanotube and nanotube/nanoclay related polymer composite materials. *Composite Part B*, vol. 37, pp.425–36.
- Moradi-Dastjerdi, R.; Foroutan, M.; Pourasghar, A.** (2013): Dynamic analysis of functionally graded nanocomposite cylinders reinforced by carbon nanotube by a mesh-free method. *Mater Des*, vol. 44, pp. 256-266.
- Okada, S.** (2007): Radial-breathing mode frequencies for nanotubes encapsulating fullerenes. *Chemical Physics Letters*, vol. 438, pp. 59–62.
- Shahab, S.; Mirzaeifar, R.; Bahai, H.** (2009): Coupled modification of natural frequencies and buckling loads of composite cylindrical panels. *International Journal of Mechanical Sciences*, vol. 51, pp. 708–717.
- Shen, H. S.** (2009): Nonlinear bending of functionally graded carbon nanotube reinforced composite plates in thermal environments. *Compos Struct*, vol. 91, pp. 9–19.
- Sladek, J.; Sladek, V.; Zhang, C.** (2003): Application of Meshless Local Petrov-Galerkin (MLPG) Method to Elastodynamic Problems in Continuously Nonhomogeneous Solids. *CMES: Computer Modeling in Engineering & Sciences*, vol. 4,

no. 6, pp. 637-647.

**Sladek, J.; Sladek, V.; Solek, P.; Tan, C.L.; Zhang, Ch.** (2009): Two- and Three-Dimensional Transient Thermoelastic Analysis by the MLPG Method. *CMES: Computer Modeling in Engineering & Sciences*, vol. 47, no. 1, pp. 61-96.

**Sladek, J.; Stanak, P.; Han, Z.D.; Sladek, V.; Atluri, S.N.** (2009): Applications of the MLPG Method in Engineering & Sciences: A Review. *CMES: Computer Modeling in Engineering & Sciences*, vol. 92, no. 5, pp. 423-475.

**Soares Jr., D.; Sladek, J.; Sladek, V.** (2009): Dynamic Analysis by Meshless Local Petrov-Galerkin Formulations Considering a Time-Marching Scheme Based on Implicit Green's Functions. *CMES: Computer Modeling in Engineering & Sciences*, vol. 50, no. 2, pp. 115-140.

**Soares Jr., D.; Sladek, J.; Sladek, V.** (2010): Non-linear dynamic analyses by meshless local Petrov-Galerkin formulations. *Int. J. Numer. Meth. Engng*, vol. 81, pp. 1687-1699.

**Talebian, S. T.; Tahani, M.; Hosseini, S. M.; Abolbashari, M. H.** (2010): Displacement time history analysis and radial wave propagation velocity in pressurized multiwall carbon nanotubes. *Computational Materials Sciences*, vol. 49, pp. 283-292.

**Talebian, S. T.; Tahani, M.; Abolbashari, M. H.; Hosseini, S. M.** (2011): Effects of dimensional parameters and various boundary conditions on axisymmetric vibrations of multiwalled carbon nanotubes using a continuum model. *Archive of Applied Mechanics*, vol. 81, pp. 1129-1140.

**Talebian, S. T.; Tahani, M.; Abolbashari, M. H.; Hosseini, S. M.** (2012): An analytical solution for thermal shock analysis of multiwall carbon nanotubes. *Computational Materials Sciences*, vol. 61, pp. 291-297.

**Thostenson, E. T.; Ren, Z. F.; Chou, T. W.** (2001): Advances in the science and technology of carbon nanotubes and their composites: a review. *Composite Science and Technology*, vol. 61, pp.1899-912.

**Uchida, T.; Tazawa, M.; Sakai, H.; Yamazaki, A.; Kobayashi, Y.** (2008): Radial breathing modes of single-walled carbon nanotubes in resonance Raman spectra at high temperature and their chiral index assignment. *Applied Surface Science*, vol. 254, pp. 7591-7595.

**Wu, X. H.; Chang, Z. J.; Lu, Y. L.; Tao, W. Q.; Shen, S. P.** (2012): An analysis of the convection-diffusion problems using meshless and meshbased methods. *Eng. Anal. Bound. Elem.*, vol. 36, pp. 1040-1048.

**Zhao, X.; Ando, Y.; Qin, L.C.; Kataura, H.; Maniwa, Y.; Saito, R.** (2002): Radial breathing modes of multiwalled carbon nanotubes. *Chemical Physics Letters*, vol. 361, pp.169–174.

